The residence time of water vapour in the atmosphere

Gimeno, Luis; Eiras-Barca, Jorge; Durán-Quesada, Ana María; Dominguez, Francina; van der Ent, Ruud; Sodemann, Harald; Sánchez-Murillo, Ricardo; Nieto, Raquel; Kirchner, James W.

DOI
10.1038/s43017-021-00181-9

Publication date
2021

Document Version
Final published version

Published in
Nature Reviews Earth and Environment

Citation (APA)
Gimeno, L., Eiras-Barca, J., Durán-Quesada, A. M., Dominguez, F., van der Ent, R., Sodemann, H., Sánchez-Murillo, R., Nieto, R., & Kirchner, J. W. (2021). The residence time of water vapour in the atmosphere. *Nature Reviews Earth and Environment*, *2*(8), 558-569. https://doi.org/10.1038/s43017-021-00181-9

The residence time of water vapour in the atmosphere

Luis Gimeno[1] ✉, *Jorge Eiras-Barca*[1,2], *Ana María Durán-Quesada*[3,4], *Francina Dominguez*[5], *Ruud van der Ent*[6], *Harald Sodemann*[7,8], *Ricardo Sánchez-Murillo*[9], *Raquel Nieto*[1] and *James W. Kirchner*[10]

Abstract | Atmospheric water vapour residence time (WVRT) is an essential indicator of how atmospheric dynamics and thermodynamics mediate hydrological cycle responses to climate change. WVRT is also important in estimating moisture sources and sinks, linking evaporation and precipitation across spatial scales. In this Review, we outline how WVRT is shaped by the interaction between evaporation and precipitation, and, thus, reflects anthropogenic changes in the hydrological cycle. Estimates of WVRT differ owing to contrasting definitions, but these differences can be reconciled by framing WVRT as a probability density function with a mean of 8–10 days and a median of 4–5 days. WVRT varies spatially and temporally in response to regional, seasonal and synoptic-scale differences in evaporation, precipitation, long-range moisture transport and atmospheric mixing. Theory predicts, and observations confirm, that in most (but not all) regions, anthropogenic warming is increasing atmospheric humidity faster than it is speeding up rates of evaporation and precipitation. Warming is, thus, projected to increase global WVRT by 3–6% K^{-1}, lengthening the distance travelled between evaporation sources and precipitation sinks. Future efforts should focus on data integration, joint measurement initiatives and intercomparisons, and dynamic simulations to provide a formal resolution of WVRT from both Lagrangian and Eulerian perspectives.

The hydrological cycle is a fundamental component of the climate system, transferring energy and mass between the atmosphere, ocean, cryosphere and land reservoirs. Despite holding less than 0.001% of all of Earth's water[1], the atmosphere acts as a key facilitator of these transfers. As such, atmospheric water vapour residence time (WVRT) is a fundamental, if not yet fully resolved, diagnostic of hydrological variability needed to estimate moisture sources and sinks[2], and understand changes in dynamic and thermodynamic processes[3], for example.

Several metrics have emerged to quantify the various facets of WVRT. These include the time in the atmosphere between evaporation and precipitation (lifetime), the age of water vapour at a specific time (AGE) and its 'life expectancy' (forward transit time, FTT) (BOX 1). Given that WVRT cannot be calculated directly, indirect methods must be used. Such methods span simple arithmetic calculations (turnover time, TUT), to those that require sophisticated moisture tracking models of various sorts (analytical, offline Eulerian or Lagrangian, or numerical tracers embedded within regional or global climate models[4,5]).

As a result of these definition-based and method-based contrasts[4–7], estimates of the global mean WVRT vary, typically ranging from 4–5 to 8–10 days[3,8–10]. In addition, it is now also recognized that there is substantial spatial variability in WVRT, owing to a combination of surface evaporation, advection, turbulent mixing, precipitation and small-scale physical processes[11]. For instance, a narrow distribution of relatively short WVRTs is anticipated in regions of intense convection (especially during summer), whereas broader distributions with longer WVRTs are expected in the polar regions (especially during winter), where evaporation and precipitation are markedly lower.

Temporal variability is also evident, not least in the long-term changes in WVRT owing to anthropogenic warming. Observations[12,13] and models[13,14], for example, suggest that warming-related increases in atmospheric moisture relative to precipitation[15] will slow the atmospheric hydrological cycle, increasing the residence time[16]. Such changes, in combination with the definition-based and method-based uncertainties, will have important implications for understanding many aspects of the hydrological cycle. For instance, any shifts in moisture holding capacity will influence precipitation extremes[17] and, in turn, the characteristics of floods and drought[18,19]. Moreover, knowledge of WVRT is critical for understanding moisture recycling, downstream impacts

✉e-mail: l.gimeno@uvigo.es

https://doi.org/10.1038/s43017-021-00181-9

Author addresses

[1]Centro de Investigación Mariña, Universidade de Vigo, Environmental Physics Laboratory (EPhysLab), Ourense, Spain.
[2]Defense University Center at the Spanish Naval Academy, Marín, Spain.
[3]Atmospheric, Oceanic and Planetary Physics Department & Climate System Observation Laboratory, School of Physics, University of Costa Rica, San José, Costa Rica.
[4]Center for Geophysical Research, University of Costa Rica, San José, Costa Rica.
[5]Department of Atmospheric Sciences, University of Illinois at Urbana-Champaign, Urbana-Champaign, IL, USA.
[6]Department of Water Management, Delft University of Technology, Delft, Netherlands.
[7]Geophysical Institute, University of Bergen, Bergen, Norway.
[8]Bjerknes Centre for Climate Research, Bergen, Norway.
[9]Stable Isotopes Research Group, Universidad Nacional de Costa Rica, Heredia, Costa Rica.
[10]Department of Environmental Systems Science, ETH Zürich, Zürich, Switzerland.

of evaporation[20,21], the intensity of the Intertropical Convergence Zone (ITCZ)[22], water vapour input to the stratosphere[23] or moisture sources for storm tracks[24], motivating in-depth assessments of WVRT.

In this Review, we synthesize current knowledge concerning WVRT and highlight it as an essential indicator of how the atmospheric hydrological cycle responds to dynamic and thermodynamic processes related to climate change. We begin by outlining how WVRT represents interactions between evaporation and precipitation, and is, thus, an indicator of hydrological cycle change. We then outline estimates of WVRT in observations and models, summarizing the uncertainty in its quantification at both global and regional scales. We subsequently analyse observed and expected changes in WVRT as a result of anthropogenic warming and end with future research priorities and pathways.

A metric of the atmospheric water cycle

The balance between evaporation and precipitation processes at local to global scales produces a range of WVRT durations. Different metrics can be related to one another using the concept of the lifetime distribution, as will now be discussed.

Box 1 | **Defining water vapour residence time**

The quantification of water vapour residence time has traditionally relied on different metrics that can result in contrasting estimates. The most common metrics used are:

Turnover time (TUT): bulk mean age of the outflow from a reservoir. For the atmosphere, TUT equals the global average mean age of precipitation. It can be calculated as $TUT = W/P$, where W is precipitable water (or water vapour) and P is precipitation.

Depletion time constant: the local calculation of W/P. Values might vary substantially from TUT, but the global precipitation weighted average is equal to TUT.

AGE: the average age of water in the atmosphere since evaporation, which can differ from precipitation age. There are indications that heterogeneity causes the global average storage weighted AGE to be slightly higher than TUT.

Backward transit time (BTT) or lifetime: the time that a precipitated water particle spends in the atmosphere.

Lifetime distribution (LTD): the probability density function of all lifetimes of BTT in a specific region or globally. The global precipitation weighted average of LTD is equal to TUT.

Forward transit time (FTT): the time that an evaporated water particle will spend in the atmosphere. In principle, BTT of a water particle at the sink location is the same as FTT of that water particle at the source location. Hence, FTT is, on average, identical to BTT or lifetime, but with different regional patterns. FTT is heavily influenced by the type of land use (FIG. 2).

Defining lifetime distribution. To the first order, the global atmosphere can be considered as an approximately steady-state reservoir for water vapour. New water vapour continuously enters the atmosphere through evaporative fluxes from the ocean and land surface, and is removed by precipitation within weather systems. In the long term, this steady-state system is in mass balance, and the fluxes into and out of the reservoir reflect the timescale of how long water vapour stays in the atmosphere. The ratio between the global bulk reservoir and corresponding fluxes then yields the average TUT (BOX 1) of about 8–10 days[3,25,26].

However, considering the global atmosphere as a homogeneous, well-mixed system is an idealization, with respect to both space and time[7]. More targeted metrics are, thus, needed to quantify the multifaceted properties of WVRT, each with different applications to the hydrological cycle[9] (BOX 1). AGE, for instance, is a distinct property of the water in the atmosphere itself. By contrast, the lifetime (or backward transit time, BTT) offers perspectives on outflow, while the FTT (or life expectancy) offers perspectives on inflow. Unless the system is continuously and completely mixed, AGE will generally differ from both FTT and BTT, even at steady state[27]. For example, in a pipe flow ('first in, first out') system, BTT will be twice the AGE, whereas in heterogeneous systems characterized by preferential flow, the outflow will be younger than the average AGE[27].

The heterogeneity of the global water cycle does not alter the mean age of precipitation (the lifetime or BTT), which remains unchanged as a result of mass balance. However, it does increase the mean AGE relative to the mean age of precipitation. The constant precipitation lifetime implies that a larger contribution of short-lived vapour that precipitates is compensated by a corresponding contribution of water vapour that does not precipitate as readily, and, thus, is longer lived. Therefore, the global and regional WVRT could be more accurately represented by a probability density function, the so-called lifetime distribution[7,9,28] (LTD; FIG. 1a).

In this framework, quantities such as the TUT and lifetime (or BTT) measure different aspects of the LTD. Global patterns of WVRT reveal lifetimes (or BTTs) of 4–5 days, markedly different from the global TUT of 8–10 days[8]. This discrepancy can be explained by noting that these BTTs are estimated by Lagrangian methods that cannot reliably capture the long and thin tail of the LTD[7]. Therefore, the BTTs reflect the median of the heavily skewed LTD, rather than its mean, which is estimated by the TUT (FIG. 1). The median of the LTD was proposed to serve as a more robust metric for the lifetime of the majority of the precipitation, since it is influenced less by the long tail than the mean of the distribution[7] (FIG. 1b). Whether the median or the mean of the LTD, the LTD itself or other quantities might be most informative has not been examined and would depend on the purpose.

Lifetime distribution variability. The LTD of different water cycle components depends on the interaction of different processes, of which atmospheric properties (saturation, boundary layer height (BLH) and transport),

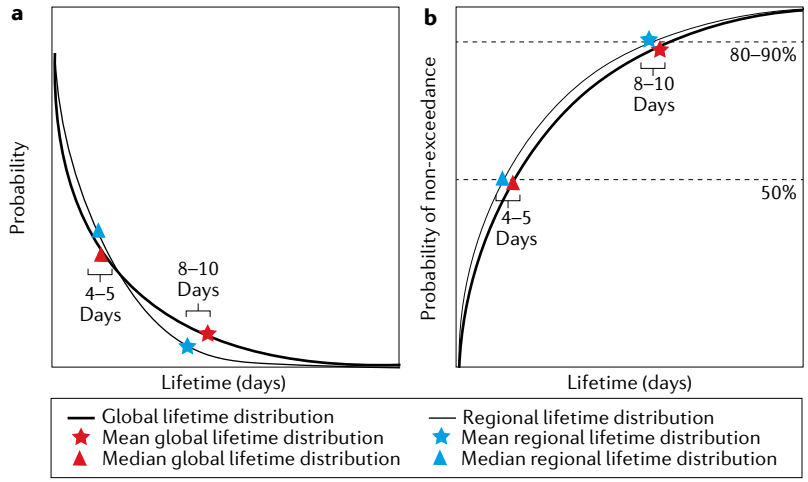

Fig. 1 | **Schematic depiction of the global lifetime distribution. a** | Probability density functions of lifetime distribution (LTD), or backward transit times depending on terminology, for the globe and a regional example with higher contribution from short-lived vapour. Triangle and star symbols denote the median and mean LTD, respectively, with the latter also representing turnover time. **b** | As in panel **a**, but the corresponding cumulative distribution function of the LTD, providing the probability of non-exceedance. While the median LTD is defined as the mid-point of the distribution, the mean LTD is found at variable locations on the upper tail (here, 80–90% of the distribution). LTDs are heavily skewed, vary regionally and can be characterized by their mean or median. Adapted from REF.[7], CC BY 4.0 (https://creativecommons.org/licenses/by/4.0/).

evaporation processes (ocean or land surface, location, land use and vegetation) and precipitation processes (circulation, weather systems and topography) are key determinants. In particular, surface–atmosphere coupling and the corresponding modulation of evaporative fluxes (governed by the boundary layer)[29] gives rise to LTDs with markedly different shapes (FIG. 2). While much is unknown about the shape of the LTD for different climates and surface properties, it has been demonstrated for precipitation extremes in the Mediterranean[11] that they vary considerably from event to event between those dominated by local and immediate moisture origin (FIG. 2a,d), long-range transport dominated with a thicker tail (FIG. 2b,c) or intermediate shapes (FIG. 2e,f).

Indeed, the boundary layer directly affects WVRT by modulating moisture exchange between the surface and the free atmosphere to balance the surface energy budget. Surface fluxes are constrained by the boundary layer and the way it responds to the large-scale atmospheric circulation. For example, evaporation increases under the presence of a drier boundary layer associated with convective development. The BLH is sensitive to the surface coupling and its growth is defined by the sensible heat flux. Hence, the BLH varies seasonally in response to the surface fluxes and also depends on the surface characteristics. In semi-arid regions, it has been demonstrated[30] that the link between the boundary layer and soil moisture features a positive feedback between deep convection and soil moisture at the storm scale (FIG. 2b). For tropical forests, observations over the Amazon reveal that BLH deepening, enhanced by increasing sensible heat flux, can aid the evolution of shallow cumulus into deep convective clouds[31] (FIG. 2c). These examples illustrate how a systematic analysis of the interrelation between BLH and free-troposphere moisture can be used to evaluate the surface–atmosphere coupling that modulates WVRT on regional scales.

Application of WVRT. Whilst being a fundamental characteristic of the regional and global turnover of water vapour in the atmosphere, WVRT also has a number of concrete applications. First, consider that the age of precipitation is inherently linked to water vapour's origins and its atmospheric transport. The concept of WVRT, thus, links the processes of evaporation, transport, mixing and precipitation at different spatial and temporal scales. This notion is especially important for rain-fed agriculture[32–34], where different water sources (and residence times) influence the occurrence of wet and dry years[35]. For example, it is conceivable that the onset of the rainy season could be characterized by relatively old atmospheric water parcels that have travelled long distances, but that, during the rainy season itself, most rainfall could be relatively young. In such a scenario, WVRT could become particularly important for water resources because the start of a drought in a given location could be linked to a lack of old water vapour from upwind, whereas the intensification of a drought could be linked to a lack of young water[36].

Another example of how WVRT pinpoints the role of a different process for the atmospheric water cycle is related to evapotranspiration. On average, moisture transpired by plants remains in the air for about one day longer than moisture evaporated from soils or canopy interception[36]. The reason for this is that, during the dry season[37], when water vapour can travel further and, thus, remains in the atmosphere longer[6], transpiration is the only evaporative flux. Regardless of origin, all evaporative processes (which, in hydrology, are generally regarded as losses from the land surface) supply precipitation elsewhere and, thus, constitute an important ecosystem service[38].

Furthermore, WVRT allows the impact of different weather systems on the atmospheric water cycle to be characterized. LTDs diagnosed for extreme precipitation events in the Mediterranean differ substantially from case to case, with medians ranging between 7.2 and 2.8 days, and modal peaks ranging between 3 h and 5 days[11]. Generally, however, their LTD resembles the global lifetime distribution (FIG. 1a), albeit with a longer tail and with seasonal variability[9]. A water vapour tagging method in a regional model yielded a lifetime of only 1–2 days for more than half of the precipitation during a cold-air outbreak in the Norwegian basin[39]. Thus, the WVRT is not only an atmospheric property but also highlights dominant turnover processes for water vapour in weather systems.

Regional estimates of WVRT

Global WVRT is, to the first approximation, dominated by the effects of large-scale atmospheric motion and oceanic evaporation on atmospheric moisture. As a result, global WVRT patterns resemble the spatial distribution of atmospheric moisture, evaporation and precipitation (FIG. 3). However, these processes do not fully explain the spatial variability of WVRT. Regional and

local-scale processes that modulate surface fluxes and precipitation (such as land-surface processes or weather systems)[6,8] exert an influence in shaping WVRT. Hence, the spatial variability of WVRT is explained by a combination of global, large-scale, regional and local-scale processes, all of which might result in shorter or longer WVRTs (and, thus, discrepancies with globally aggregated estimates).

Understanding regional differences. In general, estimates of mean and median BTT indicate substantial variations from the global mean in regions affected by large-scale vertical movement or large rainfall contrasts (FIG. 3a,b). For instance, longer BTTs are typically identified for areas influenced by the ITCZ or the South Pacific Convergence Zone, that is, the Pacific coast of Colombia and Central America and the Maritime Continent. Longer BTTs are also observed in the Sahel, where the ratio of surface evaporation to potential evapotranspiration is very small[40], as well as the Indian monsoon region. In contrast, shorter residence times occur at the descending branches of Hadley cells (subtropical highs), sharing a similar pattern with areas of enriched deuterium (FIG. 3d) and low tropical precipitation (FIG. 3e); polar highs typically exhibit higher WVRT in comparison, owing to the effect of the poleward decrease in atmospheric moisture content and in rates of precipitation and evaporation.

Evaporation from the ocean surface is the largest flux of moisture to the atmosphere. In regions with higher evaporation rates, WVRT tends to be shorter, owing to the higher moisture flux through the atmosphere. Hence, in oceanic regions with higher net radiation fluxes, WVRT is reduced as a result of enhanced evaporation. Continental regions that experience heavy rainfall, such as those affected by the ITCZ or monsoonal

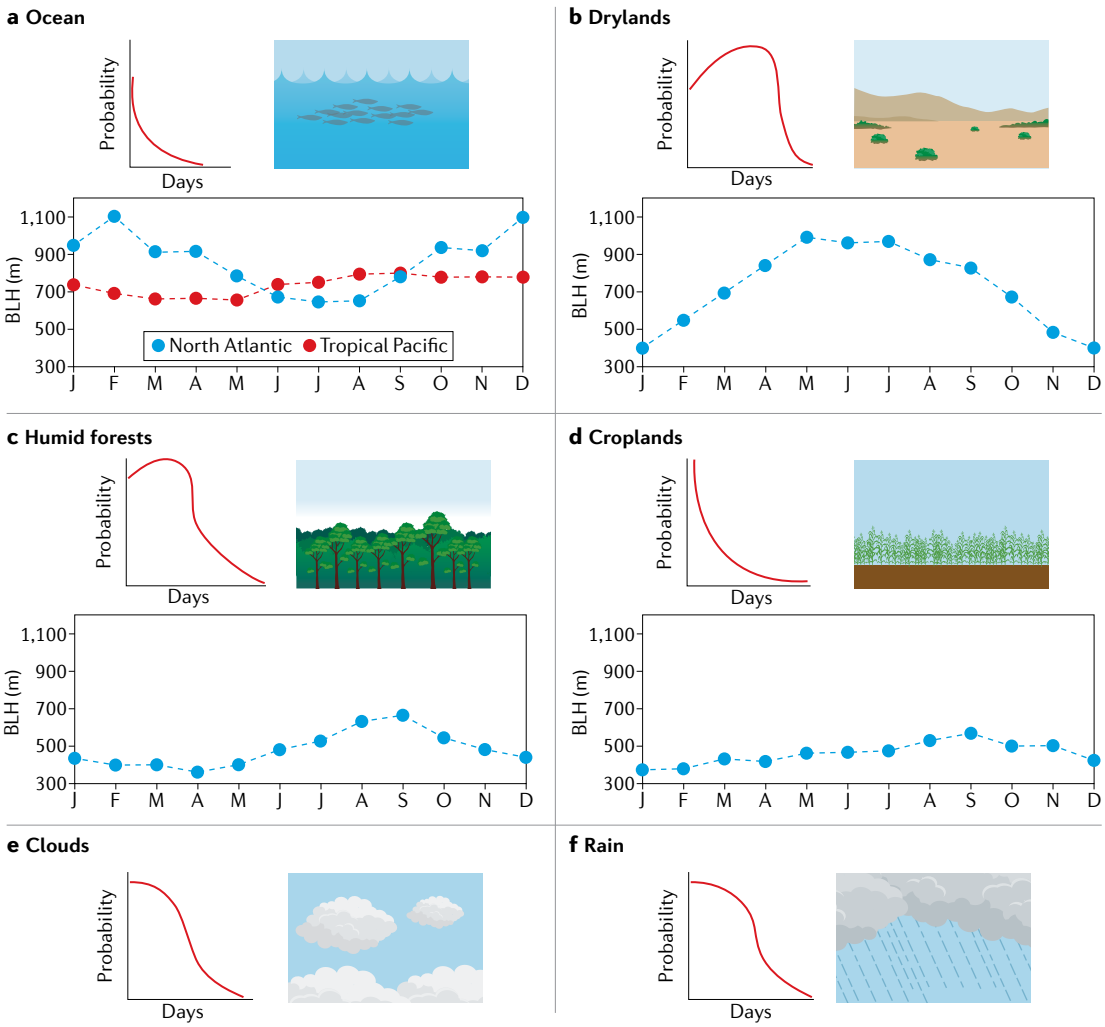

Fig. 2 | **Lifetime distribution of different surface conditions and water cycle components.** Schematic lifetime distribution (LTD) and boundary layer height (BLH) for ocean (panel **a**), drylands (panel **b**), humid forests (panel **c**), croplands (panel **d**), clouds (panel **e**) and rain (panel **f**). LTDs are roughly based on the findings of REFS[6,37]. BLH values are monthly 2019 averages from ERA5 (REF.[108]) taken over: 25°–50° N, 15°–60° W for the North Atlantic; 10° S–10° N, 100°–180° W for the Tropical Pacific; 10°–30° N, 10° W–30° E for the Sahara (drylands); 0°–20° S, 45°–70° W for the Amazon (humid forests); and 20°–35° N, 110°–120° E for Eastern China (croplands). LTD varies according to the surface conditions, responding to changes in surface fluxes or boundary layer characteristics.

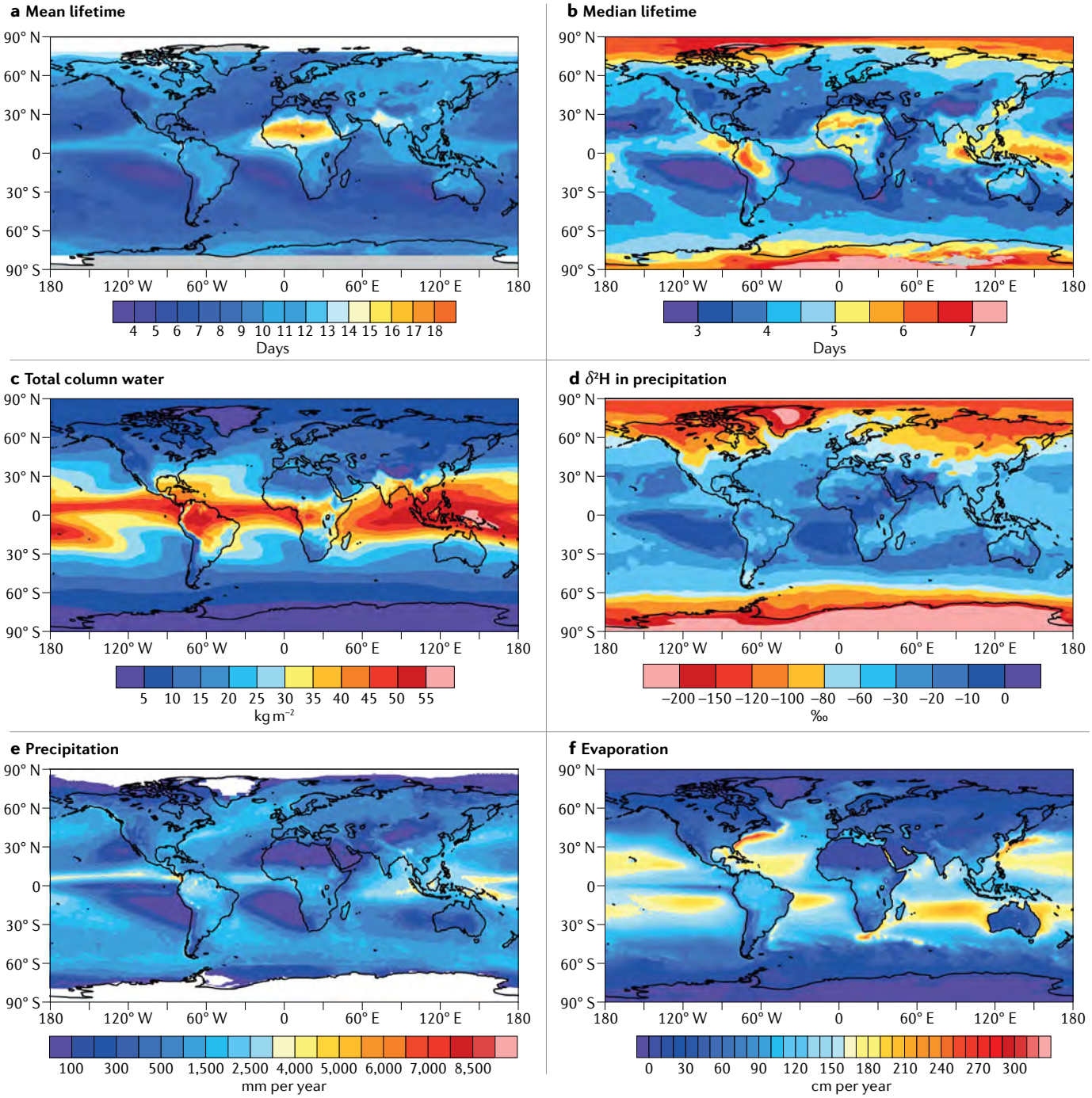

Fig. 3 | **Global patterns of water vapour residence time estimates and precipitation characteristics. a** | Annual mean lifetime or backward transit time. **b** | Annual median lifetime or backward transit time. **c** | Total column water climatology (1980–2019) from ERA5 (REF.[108]). **d** | Annual mean δ^2H in surface precipitation, as simulated by the isotope-enabled ECHAM5-WISO[109]. **e** | Annual rainfall total climatology (2001–2019) from 3IMERGM[110]. **f** | Annual evaporation climatology (1980–2019) from ERA5 (REF.[108]). The global distribution of mean and median lifetime differs owing to different processes and time scales considered. Panel **a** adapted from REF.[9], CC BY 3.0 (https://creativecommons.org/licenses/by/3.0/). Panel **b** adapted from REF.[7], CC BY 3.0 (https://creativecommons.org/licenses/by/3.0/).

circulation, tend to have longer WVRTs than oceanic regions. Convective development has a major role in determining the length of the WVRT in these terrestrial regions, and the large-scale patterns and synoptic-scale events do not fully explain the spatial and temporal variability that is observed. Tropical convection originates in the subcloud layer, where ascending and descending movements of air modulate WVRT through variations in saturation. Downdraughts during storms transport colder and drier air from the upper levels to the surface, so that an overall cooling effect after rainfall events might cause a local decrease in residence time as a direct

result of the Clausius–Clapeyron relationship. In addition, in convective regimes, re-evaporation of rainfall can contribute substantially (20–50%) to atmospheric moisture[41]. Observational evidence shows that latitudinal variations in evaporative fluxes that feed atmospheric moisture are amplified in areas prone to the development of heavy rainfall[42–44]. In such conditions, the release of latent heat dominates the cooling of air through evaporation, and, thus, WVRT is affected by condensation and evaporation simultaneously within the same air parcel.

Over land, the components of land evaporation (interception, soil evaporation and transpiration[45]) become more relevant. The magnitudes of these different fluxes are largely controlled by vegetation[46] and dominated by transpiration, which is about 60% of total land-surface evaporation[47,48]. The contribution of land evaporation to atmospheric moisture depends on local processes that are subject to large spatial variability, mainly owing to spatially heterogeneous vegetation coverage and land use. WVRT is strongly influenced by the type of land evaporation; FTTs appeared to be most skewed (towards shorter transit times) for interception and least skewed for transpiration[6]. Dry-season transpiration tends to remain in the atmosphere longer and travel farther[37]. Moreover, land evaporation is connected strongly to moisture recycling, where it contributes substantially to atmospheric moisture[49]. Because precipitation recycling influences the transfer of atmospheric moisture and modulates evaporation components through humidity and temperature changes, it is highly relevant in arid regions, where recycling accounts for a large portion of the available precipitation[34,37,50–52].

As well these broad-scale geographical differences in WVRT, specific differences are also observed at the country level. For instance, over China, BTT has been estimated at 6.3 and 8.3 days for precipitation and evaporation, respectively[53]. Moreover, annual median and mean BTTs are estimated at 4–9 days[8] and 9–12 days for a similar domain[9]. Similar disparities in WVRT estimates are also found in other regions. Over the USA, for example, WVRT has been variably estimated at 3–9 days[3], 8–11 days[9] or 4–12 days[8].

The apparent differences in the regional estimates following different estimations are most noticeable over the tropical areas (FIG. 3a,b). The median lifetime definition is able to capture the short-term moisture variations associated with synoptic-scale processes. This representation provides a more accurate estimate, as it contains the information of fast-lived changes within the hydrological cycle at the regional scale. It is consistent with the seasonality, rapid variations and spatial patterns of the atmospheric water content (FIG. 3c). At regional scales, the uncertainties in the estimation of evapotranspiration add a source of bias to the estimates of WVRT. While satellite retrievals and the advances in surface precipitation networks enable the generation of better global precipitation products, monitoring of evapotranspiration remains a challenge. Bias in the closure of energy and mass budgets might deviate WVRT estimates because of the complex transition between the local and the regional scales in terms of surface fluxes.

Water isotopes as indicators of regional WVRT. The regional differences in WVRT highlight the need to obtain independent observational metrics that can constrain different model-based estimates. Naturally occurring stable isotopes of oxygen and hydrogen that are incorporated into water molecules can provide such observational constraints[54]. The higher molecular mass of isotopically heavier water vapour molecules causes them to condense more readily. Therefore, as water is processed in atmospheric weather systems and progressively rained out, a smaller and smaller fraction of the initial concentration of heavy isotopes remains in the water vapour. This so-called isotopic fractionation can be observed with measurements taken on rainwater samples or on the water vapour itself, and with remote sensing instrumentation, including satellites[55]. It can, thus, be expected that water vapour that has travelled longer and further from its evaporation source, and undergone more uplift and cooling, to be isotopically different from the initial evaporation source. An increasing number of numerical models are capable of calculating stable isotope fractionation, creating the potential to constrain model-derived metrics of the WVRT by stable water isotope measurements[56], and also to constrain the models themselves.

The patterns of WVRT expressed as BTT reveal remarkable commonalities with the simulated stable isotope ^{2}H in surface precipitation (FIG. 3d). The relation between WVRT and isotopic composition might be most obvious with latitude, where long WVRT corresponds to the strongest loss in heavy isotopes, owing to continued condensation and fractionation with poleward moisture transport. Subtropical regions dominated by evaporation exhibit patterns that strongly resemble the areas with short WVRTs. Mid-latitude and high-latitude evaporation and land processes complicate these first-order relations, as mixing, progressive rainout of oceanic moisture and recycling with increasing continentality create a more complex signal. Regionally, patterns can even be opposite, for example, over equatorial Africa, where relatively high WVRT coincides with relatively enriched vapour isotopes.

The multifaceted relation between WVRT and stable water isotopes can be conceptualized using a schematic cross section of the atmosphere from equator to pole (FIG. 4a). Correlations of water vapour's stable isotope composition with the WVRT (expressed as AGE) are particularly obvious in the downwelling branch of the Hadley cell and in the middle troposphere of polar regions. In these regions, the transport pathways (and, thus, AGE) are longest, and cold temperatures lead to strong loss of heavy isotopes by condensation in regions where the time since evaporation is longest (FIG. 3a). For example, water vapour in the Bolivian Andes has been observed to be strongly depleted in ^{2}H (REFS[57,58]), contrasting with regions of tropical deep convection[59]. Such general patterns can also be observed from satellite sensors[41]. In extratropical regions, subarctic water vapour has been detected descending in a Mediterranean anticyclone that had experienced a loss of ^{2}H, creating a strong contrast to the water evaporating from the Mediterranean sea below[60]. Greenland vapour

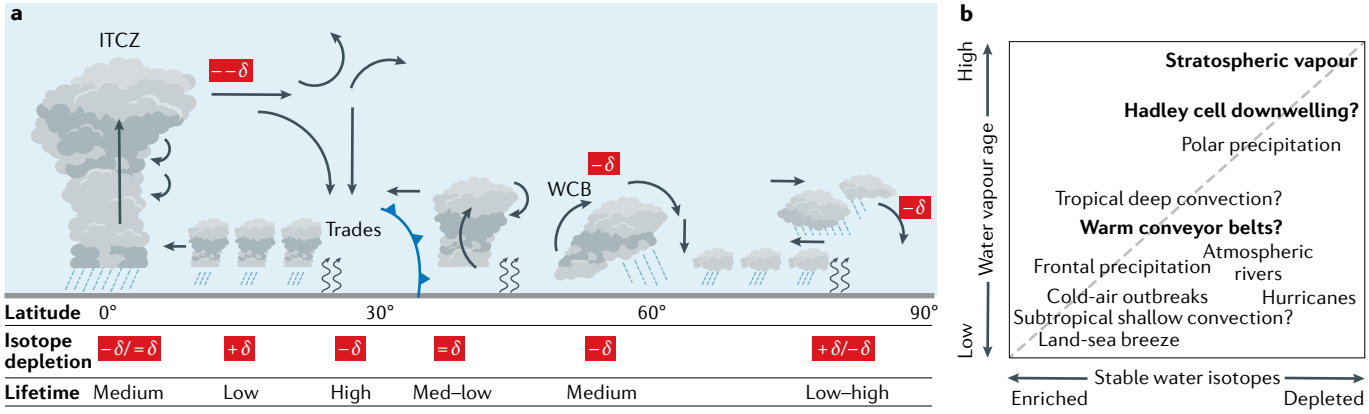

Fig. 4 | **The relation between water vapour residence time and stable isotope composition in atmospheric water vapour. a** | Schematic depiction of water vapour pathways within global weather systems (including evaporation, transport, mixing and precipitation) and their corresponding approximate lifetime and connection to loss of isotopically heavy vapour during condensation processes. **b** | Expected correspondence of lifetime to loss of heavy isotopes from weather systems that produce precipitation and residual vapour (bold). Stable water isotopic composition experiences variations during the life cycle of the rain-producing process. While subdaily samples show that synoptic systems can undergo variations across the enriched–depleted spectrum, daily and longer-term samples would provide information on the event peak. ITCZ, Intertropical Convergence Zone; WCB, warm conveyor belt.

measurements are also generally highly depleted, owing to strong orographic rise, cold temperatures and the high elevations of measurement locations[61]. On the other hand, shallow, precipitating weather systems, such as cold-air outbreaks in polar regions[21,39,62], show a signature close to the isotopic composition of vapour above the ocean[63]. Weather systems with shallow precipitation processes thus exhibit isotope signals that represent a more immediate origin and lower AGE of water vapour.

The correspondence between isotope composition in vapour and the WVRT can be synthesized in a two-dimensional diagram of AGE versus isotopic depletion (FIG. 4b). While the stable water isotopic composition of rainfall changes during the life cycle of the precipitation-producing systems and processes, the isotopic fingerprint provides information of the prevailing or dominant signal. Hence, a link between AGE and the isotopic composition of the precipitation-producing system at its peak can be established and stable water isotopes can be translated into a proportional of AGE. Atmospheric mixing of water vapour and precipitation pose substantial challenges to obtaining such observational constraints on the WVRT. For example, tracing aged water vapour during mixing processes is hampered by the abundance of moist air near the surface that will, by far, outweigh the isotopic signal contained in the aged water vapour. In addition, rainfall continuously exchanges mass with the surrounding vapour phase as it falls through the atmospheric column below the cloud base in a complex mixing process that also entails isotopic fractionation[64]. Both of these aspects suggest that water vapour lifetime might, to some extent, remain a conceptual quantity with large uncertainties in both tails of its distribution.

Using the combination of stable isotopes of both hydrogen and oxygen in water vapour, it is possible to calculate an evaporation source tracer that could be used to trace water vapour and quantify mixing processes[65]. This 'deuterium excess' could provide proxy information about the WVRT and also information about moisture recycling and transpiration ratios[66–68]. Moreover, the use of water isotopes is not limited to atmospheric processes, as they have also been widely used to track surface and subsurface hydrological processes[69–71].

WVRT and anthropogenic climate change

As well as the previously described regional variability in WVRT, influenced by local-to-global scale processes, WVRT is also anticipated to change with anthropogenic warming. The dependence of TUT (BOX 1) on temperature provides a means by which the sensitivity of WVRT to future warming can be assessed. In particular, if $\varphi_{\overline{W}}$ and $\varphi_{\overline{P}}$ represent the fractional rate of change of vertically integrated precipitable water ($\overline{W}$) and precipitation rate ($\overline{P}$), respectively, with units of K^{-1}, the equivalent rate of change in residence time can be derived as:

$$\varphi_{\overline{W}} = \frac{1}{\overline{W}}\frac{\partial \overline{W}}{\partial \overline{T}} \quad (1)$$

$$\varphi_{\overline{P}} = \frac{1}{\overline{P}}\frac{\partial \overline{P}}{\partial \overline{T}} \quad (2)$$

$$\varphi_{\mathrm{TUT}} = \frac{1}{\mathrm{TUT}}\frac{\partial \mathrm{TUT}}{\partial \overline{T}} = \frac{\overline{P}}{\overline{W}}\frac{\partial}{\partial \overline{T}}\left[\frac{\overline{W}}{\overline{P}}\right] = \varphi_{\overline{W}} - \varphi_{\overline{P}} \quad (3)$$

Alternatively, the intensity of the atmospheric hydrological cycle can be estimated through the fraction of mass exchange per unit time, defined as $M = \overline{P}/\overline{W}$ (REFS[13,14,72]). As the inverse of TUT, M is a measure of the rate at which water vapour moves through the atmospheric reservoir, with the rate of change with temperature derived as:

$$\varphi_{\mathrm{TUT}} = M\frac{\partial}{\partial \overline{T}}\left(\frac{1}{M}\right) = -\varphi_{M} \quad (4)$$

Using these relationships, the impact of anthropogenic warming on $\overline{W}$ and $\overline{P}$, and, in turn, TUT, collectively suggest a consistent increase in WVRT[13,72–78] (FIG. 5; TABLE 1), as will now be discussed.

Changes in precipitable water. Assuming that relative humidity remains constant[79], the sensitivity of $\overline{W}$ to temperature is driven by the dependence of saturation vapour pressure on temperature[80]. Thus, changes in $\overline{W}$ are approximately scaled by the Clausius–Clapeyron rate of 7% K^{-1}. Indeed, both general circulation model (GCM)-based[13,16,72–78,81,82] and satellite-based[12,13,83,84] estimates converge on column-integrated water vapour increasing at this rate (FIG. 5; TABLE 1). Such findings are particularly applicable over oceanic regions, where the assumption of constant relative humidity is most valid, but they would also likely apply at the global scale[82]. Fingerprinting methods further indicate that the observed increase in total and upper-tropospheric atmospheric moisture content can be attributed to human-induced greenhouse gas increases[81,85], although the Atlantic Multi-decadal Oscillation and El Niño–Southern Oscillation also have a distinct influence on twentieth century variability[78].

Yet, while global trends in water vapour are robustly positive, substantial geographical variability exists for both observed and projected precipitable water changes. For instance, positive W trends have been observed over the North Pacific, North Atlantic and along the ITCZ, while very weak and even negative trends are apparent in the subtropics and over other oceanic regions[12,13,84]. More generally, observational data since 1988 suggest rates of change of 4–7% K^{-1}, 10–14% K^{-1} and well below 7% K^{-1} for oceans poleward of 30°, tropical oceans and land areas, respectively[86]. In addition, expectations of homogeneous changes with altitude might also not be realistic. The majority of the observed increase in water mass, for example, occurs below 500 hPa, even when the percentage change per K is greater above that level[77]. Moreover, in contrast to column-integrated W, surface W is projected to decrease in the future over continental areas, owing to surface relative humidity changes[82].

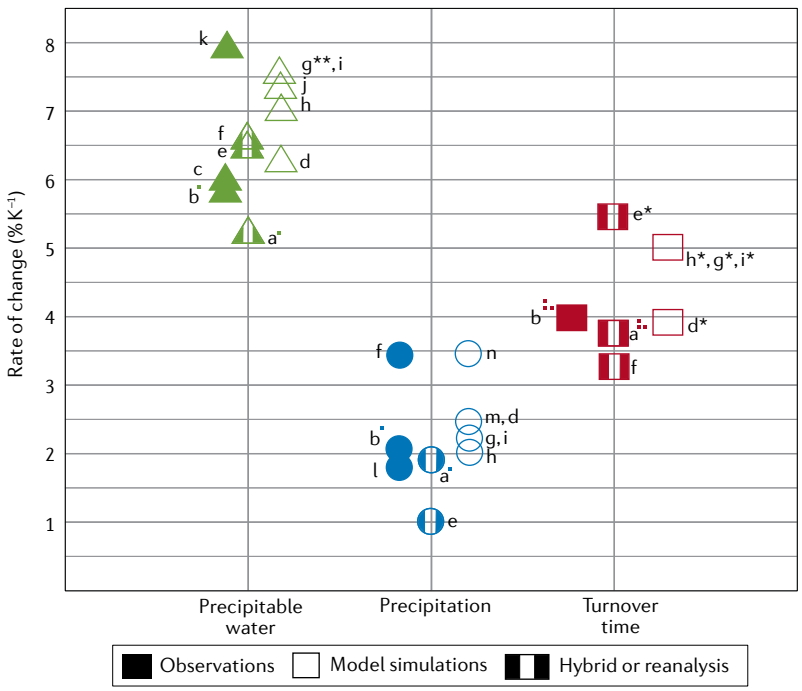

Fig. 5 | **Sensitivity of water vapour residence time and its components to global temperature.** Rate of change per degree warming for precipitable water (green), precipitation (blue) and turnover time (red). Where needed, turnover time was converted to units % K^{-1}. *Derived from changes in global precipitable water and precipitation. **Results from AR4 models. ■Derived from % per decade, with a warming reference of 0.17 K per decade. ■■Derived from recycling rate. a = REF.[13]; b = REF.[12]; c = REF.[83]; d = REF.[74]; e = REF.[78]; f = REF.[75]; g = REF.[77]; h = REF.[73]; i = REF.[72]; j = REF.[82]; k = REF.[84]; l = REF.[107]; m = REF.[88]; n = REF.[87]. Note, results from REF.[111] are not included, owing to problems with the underlying precipitation data. Most estimates, whether observational, modelled or hybrid, converge on rates of change close to 7% K^{-1} for global precipitable water, 2.5% K^{-1} for global precipitations and about 4.5% K^{-1} for turnover time.

Changes in precipitation. Estimates from GCMs typically converge on global mean precipitation increases of 1–4% K^{-1} (REFS[13,72–75,77,78,82,87,88]) (FIG. 5; TABLE 1). These predicted changes do not scale with Clausius–Clapeyron (and are, thereby, lower than those for $\overline{W}$), owing to global average precipitation being constrained by energy balance and not moisture availability[77,87]. Uncertainties in such model projections are generally represented by the spread of the model, but these are likely to be underestimates because any future precipitation responses probably encompass a much larger range[87]. However, while GCMs indicate consensus in precipitation changes, global trends from observations lack statistical significance, with most reported values ranging from 2 to 3.5% K^{-1} (FIG. 5; TABLE 1), owing, in part, to the absence of complete, reliable and consistent data products. Precipitation is also expected to respond differently to the various drivers of anthropogenic warming, resulting in fast and slow responses, which further complicate observational analyses[89].

As with W, the regional response of precipitation to warming also shows strong spatial heterogeneity. GCMs project increasing precipitation near the equator and in the mid-latitudes, while a reduction is projected in subtropical subsidence regions[90]. This pattern is also reflected in the geographical distribution of precipitation-minus-evaporation, where, over the oceans, wet regions become wetter and dry regions drier[72]. In contrast, over the continents, a more heterogeneous pattern is projected, with precipitation-minus-evaporation changes coupled to spatial patterns in surface warming and relative humidity[91–93]. Such model-derived estimates are also generally supported by observations, including increased precipitation over the ITCZ and storm-track regions, and decreased precipitation over the subtropics[13].

With the increase in available atmospheric moisture, as previously discussed, extreme precipitation is also anticipated to increase[87]. The rate of such projected changes exceeds that of mean precipitation, generally within the range of 5–10% K^{-1} in both observations[94] and GCMs[75]. Changes in short-duration extreme rainfall exceed those expected from moisture increases alone, and are likely related to feedbacks in convective clouds occurring at small scales[95].

Table 1 | **Published rates of change for turnover time, precipitation and precipitable water**

Source	TUT (% K^{-1})	Global *P* (% K^{-1})	Global *W* (% K^{-1})	Ref.
GPCP, MSAP	–	1.5–2	–	107
GPCP, SSM/I	3.85 ± 3.00[a,b]	1.94 ± 3.18[a]	5.70 ± 2.18[a]	12
SSM/I	–	–	7.8	84
MSU, AVHRR, SSM/I	–	–	6.03[c]	83
GPCP, SSM/I, CMIP5	3.70 ± 2.35[a,b]	1.82 ± 2.82[a]	5.29 ± 1.94[a]	13
GPCP, SSM/I, ERA-In, HadCRUT	3.20 ± 0.53[d]	3.40 ± 0.90	6.60 ± 0.40	75
20CRv2m HadISST, SSM/I, AR4	5.4	1	6.4	78
Ensemble of 19 AOGCMs	–	3.4	–	87
HadGEM1+	–	2–3	–	88
PCMDI/AR4	5.3[d]	2.2	7.5	72
PDRMIP, CMIP5	5.73 ± 0.81[e]	–	–	16
KCM (ECHAM5+NEMO)	~5[d]	~2	~7	73
CMIP3	–	–	7.3	82
Multiple GCMs	3.7[d]	2.5	6.2	74
AR4 models	5.1[d]	2.3	7.4	77

Standard errors were provided by authors or obtained by uncertainty propagation. *P*, precipitation; TUT, turnover time; *W*, precipitable water. [a]Derived from per decade. [b]Derived from recycling rate. [c]Averaged from 6.8% K^{-1} (20°–60° N), 6.7% K^{-1} (20° S–20° N) and 4.6% K^{-1} (20°–60° S). [d]Derived from *W* and *P*. [e]Derived from days K^{-1}, value calculated for the future period with a reference TUT of 8.2 ± 0.5 days.

Changes in WVRT. Having quantified the sensitivity of *W* and *P* to temperature increases, changes in TUT can be inferred.

All evidence points towards a lengthening of TUT with anthropogenic warming. GCMs, for example, typically reveal an increase in TUT of 3–6% K^{-1} (REFS[13,72–75,77,78]) (FIG. 5; TABLE 1). In absolute terms, these reflect a 1.7-day increase over 1986–2005 (8.2 ± 0.5 days) to 2081–2100 (9.9 ± 0.7) based on RCP8.5 projections[16]. Water vapour tracers embedded within GCMs also indicate increases in WVRT as sea surface temperatures and greenhouse gases increase with mean values of 0.13 days per 50 years over 1949–1998 and 0.3 days per 50 years over 1974–1998 (REF.[14]). These general findings are further confirmed by observational analyses of *M* (the fractional mass exchange per unit time; Eq. (4)), which indicate a decrease in *M* of −0.73% per decade on average from 1988 to 2009, implying a corresponding global increase in TUT[12,13].

As expected, changes in TUT are heterogeneous in space. For example, observations and models suggest an increase in *M* (or decrease in TUT) over the ITCZ and storm tracks, but a decrease in *M* (or increase in TUT) over the subtropics[12,13]. These geographical variations reflect those observed for precipitation. The global increase in TUT implies that the global signal is dominated by regions where residence time is increasing. Thus, global trends in TUT are dominated by trends in water vapour, while regional trends are dominated by trends in precipitation[12,13].

There is, therefore, an overwhelming consensus that, as the climate warms, WVRT increases: water vapour remains in the atmosphere for longer and a smaller fraction of this vapour is exchanged with the surface per unit of time (FIG. 5; TABLE 1). A longer WVRT implies that water vapour travels further between the evaporation source and precipitation sink, and, thus, that the length scale of moisture transport increases[96], with estimates converging on a TUT change close to 4% K^{-1}. Perhaps counter-intuitively, this lengthening occurs simultaneously with an increase in mean precipitation and evapotranspiration[14,97], an overall increased intensity of extreme precipitation[87] and increased intensity of droughts and floods[72,91]. Extreme precipitation events are often fed by the convergence of moisture from both local and remote sources[11,98,99], implying that extreme precipitation will often be a mixture of 'newer' (local) water and 'older' (more remote) water, resulting in a bimodal age distribution. Clearly, a simple measure such as TUT cannot capture such distributions or their changes in a warming climate.

Summary and future perspectives

The time water spends in the atmosphere, or WVRT, is a fundamental diagnostic of the climate system. WVRT varies widely, ranging from less than 2 days over the subtropical oceans to more than 10 days at high latitudes, reflecting regional differences in precipitation-generating mechanisms. At the global scale, estimates of residence time range from 8–10 days[3,9] to a much shorter 4–5 days[8]. These apparently contradictory estimates can be reconciled by recognizing that the atmosphere hosts a continuum of lifetimes represented by the LTD[7]. The TUT of 8–10 days thus becomes a single number that characterizes only the mean of the LTD, whereas the shorter 4–5-day estimate represents the median. As the climate warms, TUT will likely increase by 3–6% K^{-1}, lengthening the atmospheric branch of the water cycle.

Simple metrics such as TUT provide limited insight into WVRT processes. However, quantification of the changes in LTD would, for example, provide insight

in terms of increased skewness of the distribution that could reflect both more intense precipitation and more long-lived water vapour. Reconsidering previous WVRT analyses from the perspective of LTD's might, therefore, be valuable and can motivate research into identifying the LTD from models and observations.

It is clear, however, that atmospheric scientists can learn valuable lessons from other disciplines. In hydrology, for example, stable isotopes and geochemical tracers have brought about a shift from bulk quantification of the water balance to a more nuanced understanding of the physical processes and pathways of water[100]. The traditional understanding of the subsurface and surface hydrologic system was effectively reconceptualized by these observations[101,102]. Hydrologists have moved beyond mean transit times (metrics such as TUT) and have been thinking in terms of transit time distributions (LTD) for decades[103,104]. Similarly, combining isotopic tracer observations and numerical models is likely to advance understanding of WVRT in the atmosphere.

Bringing together in situ isotopic measurements, remote sensing observations and isotope-enabled models can help us bridge spatial and temporal scales as seen, for example, with the potentially improved parameterization of vertical mass exchange in climate models[56]. However, the use of isotope tracers in the atmosphere is not straightforward, as moisture sources and sinks evolve with the location of frontal and/or convective weather systems, and the isotopic signal continuously evolves from mixing and phase changes. Nevertheless, stable water isotopes in the atmosphere are currently the only quantitative tool for observing some aspects of the LTD. The community would benefit from isotopic observations and modelling aimed at constraining the LTD of water vapour in the atmosphere. Targeted observational campaigns need to be adapted to study how the LTD varies from the ITCZs to subtropics, mid-latitudes and polar regions. Ideally, such campaigns should cover an entire local or regional water cycle, from evaporation to mixing, cloud processes and precipitation. Doing so requires a focus on specific regional weather systems and a combination of measurement platforms, including research aircraft, ships, stations with flux towers, collection of precipitation and sampling of soil moisture and plants[105,106].

An outstanding challenge remains with regard to how isotope-derived information can be used on WVRT to infer the spatial origins of moisture and precipitation, as well as to differentiate between moisture and precipitation that originate from ocean evaporation, soil evaporation and transpiration. As such, observational campaigns could ideally span transects between regions where water vapour primarily originates from oceanic versus terrestrial sources. These campaigns should encompass simultaneous observations of both atmospheric and surface processes, because their interactions are poorly understood.

Advancing understanding of WVRT and its changes in response to warming will require both comprehensive measurement campaigns and tracer-enabled atmospheric models. Priorities for future work include more comprehensively documenting regional and local-scale processes, improved understanding of surface–atmosphere interactions and further development of the LTD as an organizing concept for WVRT. The complexity of these problems and their connectivity across scales will require multidisciplinary approaches drawing on broad expertise in both atmospheric science and land–ocean–atmosphere interactions.

Published online: 13 July 2021

1. Trenberth, K. E., Smith, L., Qian, T., Dai, A. & Fasullo, J. Estimates of the global water budget and its annual cycle using observational and model data. *J. Hydrometeorol.* **8**, 758–769 (2007).
2. Nieto, R. & Gimeno, L. A database of optimal integration times for Lagrangian studies of atmospheric moisture sources and sinks. *Sci. Data* **6**, 59 (2019).
3. Trenberth, K. E. Atmospheric moisture residence times and cycling: Implications for rainfall rates and climate change. *Clim. Change* **39**, 667–694 (1998).
4. Gimeno, L. et al. Oceanic and terrestrial sources of continental precipitation. *Rev. Geophys.* **50**, RG4003 (2012).
5. Dominguez, F., Hu, H. & Martinez, J. Two-layer dynamic recycling model (2L-DRM): learning from moisture tracking models of different complexity. *J. Hydrometeorol.* **21**, 3–16 (2020).
6. Tuinenburg, O. & van der Ent, R. Land surface processes create patterns in atmospheric residence time of water. *J. Geophys. Res. Atmos.* **124**, 583–600 (2019).
7. Sodemann, H. Beyond turnover time: constraining the lifetime distribution of water vapor from simple and complex approaches. *J. Atmos. Sci.* **77**, 413–433 (2020).
8. Läderach, A. & Sodemann, H. A revised picture of the atmospheric moisture residence time. *Geophys. Res. Lett.* **43**, 924–933 (2016).
9. van der Ent, R. J. & Tuinenburg, O. A. The residence time of water in the atmosphere revisited. *Hydrol. Earth Syst. Sci.* **21**, 779–790 (2017).
10. Numaguti, A. Origin and recycling processes of precipitating water over the Eurasian continent: Experiments using an atmospheric general circulation model. *J. Geophys. Res. Atmos.* **104**, 1957–1972 (1999).
11. Winschall, A., Sodemann, H., Pfahl, S. & Wernli, H. How important is intensified evaporation for Mediterranean precipitation extremes? *J. Geophys. Res. Atmos.* **119**, 5240–5256 (2014).
12. Li, L. et al. The recycling rate of atmospheric moisture over the past two decades (1988–2009). *Environ. Res. Lett.* **6**, 034018 (2011).
13. Kao, A. et al. A comparative study of atmospheric moisture recycling rate between observations and models. *J. Clim.* **31**, 2389–2398 (2018).
14. Bosilovich, M. G., Schubert, S. D. & Walker, G. K. Global changes of the water cycle intensity. *J. Clim.* **18**, 1591–1608 (2005).
15. Allan, R. et al. Advances in understanding large-scale responses of the water cycle to climate change. *Ann. N. Y. Acad. Sci.* **1472**, 49–75 (2020). **Addresses the challenges in better understanding the sensitivity of the water cycle to climate change.**
16. Hodnebrog, Ø. et al. Water vapour adjustments and responses differ between climate drivers. *Atmos. Chem. Phys.* **19**, 12887–12899 (2019).
17. Liu, B. et al. Global atmospheric moisture transport associated with precipitation extremes: Mechanisms and climate change impacts. *Wiley Interdiscip. Rev. Water* **7**, e1412 (2020).
18. Hoerling, M. & Kumar, A. The perfect ocean for drought. *Science* **299**, 691–694 (2003).
19. Winschall, A., Pfahl, S., Sodemann, H. & Wernli, H. Impact of North Atlantic evaporation hot spots on southern Alpine heavy precipitation events. *Q. J. R. Meteorol. Soc.* **138**, 1245–1258 (2012).
20. Fremme, A. & Sodemann, H. The role of land and ocean evaporation on the variability of precipitation in the Yangtze River valley. *Hydrol. Earth Syst. Sci.* **23**, 2525–2540 (2019).
21. Aemisegger, F. & Papritz, L. A climatology of strong large-scale ocean evaporation events. Part I: Identification, global distribution, and associated climate conditions. *J. Clim.* **31**, 7287–7312 (2018).
22. Byrne, M. P., Pendergrass, A. G., Rapp, A. D. & Wodzicki, K. R. Response of the intertropical convergence zone to climate change: Location, width, and strength. *Curr. Clim. Change Rep.* **4**, 355–370 (2018).
23. Mote, P. W. et al. An atmospheric tape recorder: The imprint of tropical tropopause temperatures on stratospheric water vapor. *J. Geophys. Res. Atmos.* **101**, 3989–4006 (1996).
24. Pfahl, S. & Sodemann, H. What controls deuterium excess in global precipitation? *Clim. Past* **10**, 771–781 (2014).
25. Savenije, H. Water scarcity indicators; the deception of the numbers. *Phys. Chem. Earth B: Hydrol. Oceans Atmos.* **25**, 199–204 (2000).
26. Bodnar, R. J. et al. Whole Earth geohydrologic cycle, from the clouds to the core: The distribution of water in the dynamic Earth system. *Geol. Soc. Am. Spec. Pap.* **500**, 431–61 (2013).
27. Berghuijs, W. R. & Kirchner, J. W. The relationship between contrasting ages of groundwater and streamflow. *Geophys. Res. Lett.* **44**, 8925–8935 (2017).
28. Yoshimura, K., Oki, T., Ohte, N. & KANAE, S. Colored moisture analysis estimates of variations in 1998 Asian monsoon water sources. *J. Meteorol. Soc. Japan. Ser. II* **82**, 1315–1329 (2004).
29. Van Heerwaarden, C. C., Vilà-Guerau de Arellano, J., Gounou, A., Guichard, F. & Couvreux, F. Understanding the daily cycle of evapotranspiration: A method to quantify the influence of forcings and feedbacks. *J. Hydrometeorol.* **11**, 1405–1422 (2010).
30. Taylor, C., Ellis, R., Parker, D., Burton, R. & Thorncroft, C. Linking boundary-layer variability with convection: a case-study from jet2000. *Q. J. Royal Meteorol. Soc.* **129**, 2233–2253 (2003).
31. Henkes, A., Fisch, G., Toledo Machado, L. A. & Chaboureau, J.-P. Morning boundary layer conditions

for shallow to deep convective cloud evolution during the dry season in the central amazon [preprint]. *Atmos. Chem. Phys. Discuss.* https://doi.org/10.5194/acp-2021-87 (2021).
32. Keys, P. et al. Analyzing precipitationsheds to understand the vulnerability of rainfall dependent regions. *Biogeosci. Discuss.* **8**, 10487 (2011).
33. Bagley, J. E., Desai, A. R., Dirmeyer, P. A. & Foley, J. A. Effects of land cover change on moisture availability and potential crop yield in the world's breadbaskets. *Environ. Res. Lett.* **7**, 014009 (2012).
34. Miralles, D. G. et al. Contribution of water-limited ecoregions to their own supply of rainfall. *Environ. Res. Lett.* **11**, 124007 (2016).
35. Guo, L. et al. Moisture sources for East Asian precipitation: Mean seasonal cycle and interannual variability. *J. Hydrometeorol.* **20**, 657–672 (2019).
36. Miralles, D. G., Gentine, P., Seneviratne, S. I. & Teuling, A. J. Land–atmospheric feedbacks during droughts and heatwaves: state of the science and current challenges. *Ann. N. Y. Acad. Sci.* **1436**, 19 (2019).
37. Van der Ent, R., Wang-Erlandsson, L., Keys, P. W. & Savenije, H. Contrasting roles of interception and transpiration in the hydrological cycle–Part 2: Moisture recycling. *Earth Syst. Dyn.* **5**, 471–489 (2014).
38. Keys, P. W., Wang-Erlandsson, L. & Gordon, L. J. Revealing invisible water: moisture recycling as an ecosystem service. *PLoS One* **11**, e0151993 (2016).
39. Papritz, L. & Spengler, T. A Lagrangian climatology of wintertime cold air outbreaks in the Irminger and Nordic Seas and their role in shaping air–sea heat fluxes. *J. Clim.* **30**, 2717–2737 (2017).
40. Or, D. & Lehmann, P. Surface evaporative capacitance: How soil type and rainfall characteristics affect global-scale surface evaporation. *Water Resour. Res.* **55**, 519–539 (2019).
41. Worden, J., Noone, D. & Bowman, K. Importance of rain evaporation and continental convection in the tropical water cycle. *Nature* **445**, 528–532 (2007).
42. Steen-Larsen, H. et al. Moisture sources and synoptic to seasonal variability of North Atlantic water vapor isotopic composition. *J. Geophys. Res. Atmos.* **120**, 5757–5774 (2015).
43. Bonne, J.-L. et al. Resolving the controls of water vapour isotopes in the atlantic sector. *Nature Commun.* **10**, 1632 (2019).
44. Wei, Z. et al. A global database of water vapor isotopes measured with high temporal resolution infrared laser spectroscopy. *Sci. Data* **6**, 180302 (2019).
45. Miralles, D. G., Brutsaert, W., Dolman, A. J. & Gash, J. H. On the use of the term "evapotranspiration". *Water Resour. Res.* **56**, e2020WR028055 (2020).
46. Wang, L., Good, S. P. & Caylor, K. K. Global synthesis of vegetation control on evapotranspiration partitioning. *Geophys. Res. Lett.* **41**, 6753–6757 (2014).
47. Coenders-Gerrits, A. et al. Uncertainties in transpiration estimates. *Nature* **506**, E1–E2 (2014).
48. Schlesinger, W. H. & Jasechko, S. Transpiration in the global water cycle. *Agric. For. Meteorol.* **189**, 115–117 (2014).
49. Yu, Y. et al. Observed positive vegetation-rainfall feedbacks in the Sahel dominated by a moisture recycling mechanism. *Nature Commun.* **8**, 1873 (2017).
50. Hu, H. & Dominguez, F. Evaluation of oceanic and terrestrial sources of moisture for the North American monsoon using numerical models and precipitation stable isotopes. *J. Hydrometeorol.* **16**, 19–35 (2015).
51. Li, R. & Wang, C. Precipitation recycling using a new evapotranspiration estimator for Asian-African arid regions. *Theor. Appl. Climatol.* **140**, 1–13 (2020).
52. Notaro, M., Wang, F. & Yu, Y. Elucidating observed land surface feedbacks across sub-Saharan Africa. *Clim. Dyn.* **53**, 1741–1763 (2019).
53. Wang, N., Zeng, X.-M., Zheng, Y., Zhu, J. & Jiang, S. The atmospheric moisture residence time and reference time for moisture tracking over China. *J. Hydrometeorol.* **19**, 1131–1147 (2018).
54. Gat, J. R. Oxygen and hydrogen isotopes in the hydrologic cycle. *Annu. Rev. Earth Planet. Sci.* **24**, 225–262 (1996).
55. Galewsky, J. et al. Stable isotopes in atmospheric water vapor and applications to the hydrologic cycle. *Rev. Geophys.* **54**, 809–865 (2016).
56. Aggarwal, P. K. et al. Stable isotopes in global precipitation: A unified interpretation based on atmospheric moisture residence time. *Geophys. Res. Lett.* **39**, L11705 (2012).
Showed that the interpretation based on moisture residence time is a key factor in the use of stable isotopes in precipitation to monitor impacts of past climate changes.
57. Galewsky, J. & Samuels-Crow, K. Water vapor isotopic composition of a stratospheric air intrusion: Measurements from the Chajnantor Plateau, Chile. *J. Geophys. Res. Atmos.* **119**, 9679–9691 (2014).
58. Galewsky, J. & Samuels-Crow, K. Summertime moisture transport to the southern South American Altiplano: Constraints from in situ measurements of water vapor isotopic composition. *J. Clim.* **28**, 2635–2649 (2015).
59. Hanisco, T. F. Observations of deep convective influence on stratospheric water vapor and its isotopic composition. *Geophys. Res. Lett.* **34**, L04814 (2007).
60. Sodemann, H. et al. The stable isotopic composition of water vapour above Corsica during the HyMeX SOP1 campaign: insight into vertical mixing processes from lower-tropospheric survey flights. *Atmos. Chem. Phys.* **17**, 6125–6151 (2017).
61. Steen-Larsen, H. C. et al. Continuous monitoring of summer surface water vapor isotopic composition above the Greenland Ice Sheet. *Atmos. Chem. Phys.* **13**, 4815–4828 (2013).
62. Aemisegger, F. & Sjolte, J. A climatology of strong large-scale ocean evaporation events. Part II: Relevance for the deuterium excess signature of the evaporation flux. *J. Clim.* **31**, 7313–7336 (2018).
63. Araguás-Araguás, L., Froehlich, K. & Rozanski, K. Deuterium and oxygen-18 isotope composition of precipitation and atmospheric moisture. *Hydrol. Process.* **14**, 1341–1355 (2000).
64. Graf, P., Wernli, H., Pfahl, S. & Sodemann, H. A new interpretative framework for below-cloud effects on stable water isotopes in vapour and rain. *Atmos. Chem. Phys.* **19**, 747–765 (2019).
65. Bonne, J.-L. et al. The summer 2012 Greenland heat wave: In situ and remote sensing observations of water vapor isotopic composition during an atmospheric river event. *J. Geophys. Res. Atmos.* **120**, 2970–2989 (2015).
66. Froehlich, K. et al. Deuterium excess in precipitation of Alpine regions–moisture recycling. *Isotopes Environ. Health Stud.* **44**, 61–70 (2008).
67. Aemisegger, F. et al. Deuterium excess as a proxy for continental moisture recycling and plant transpiration. *Atmos. Chem. Phys.* **14**, 4029–4054 (2014).
68. Wei, Z. & Lee, X. The utility of near-surface water vapor deuterium excess as an indicator of atmospheric moisture source. *J. Hydrol.* **577**, 123923 (2019).
69. Penna, D. et al. Tracing ecosystem water fluxes using hydrogen and oxygen stable isotopes: challenges and opportunities from an interdisciplinary perspective. *Biogeosci. Discuss.* https://doi.org/10.5194/bg-2018-286 (2018).
70. Sprenger, M. et al. The demographics of water: A review of water ages in the critical zone. *Rev. Geophys.* **57**, 800–834 (2019).
71. Jasechko, S. Global isotope hydrogeology—Review. *Rev. Geophys.* **57**, 835–965 (2019).
72. Held, I. M. & Soden, B. J. Robust responses of the hydrological cycle to global warming. *J. Clim.* **19**, 5686–5699 (2006).
73. Khon, V., Park, W., Latif, M., Mokhov, I. & Schneider, B. Response of the hydrological cycle to orbital and greenhouse gas forcing. *Geophys. Res. Lett.* **37**, L19705 (2010).
74. O'Gorman, P. A. & Schneider, T. The hydrological cycle over a wide range of climates simulated with an idealized GCM. *J. Clim.* **21**, 3815–3832 (2008).
75. O'Gorman, P. A., Allan, R. P., Byrne, M. P. & Previdi, M. Energetic constraints on precipitation under climate change. *Surv. Geophys.* **33**, 585–608 (2012).
76. O'Gorman, P. A. Sensitivity of tropical precipitation extremes to climate change. *Nat. Geosci.* **5**, 697–700 (2012).
77. Stephens, G. L. & Ellis, T. D. Controls of global-mean precipitation increases in global warming GCM experiments. *J. Clim.* **21**, 6141–6155 (2008).
78. Zhang, L., Wu, L. & Gan, B. Modes and mechanisms of global water vapor variability over the twentieth century. *J. Clim.* **26**, 5578–5593 (2013).
79. Sherwood, S., Roca, R., Weckwerth, T. & Andronova, N. Tropospheric water vapor, convection, and climate. *Rev. Geophys.* **48**, RG2001 (2010).
80. Gu, G. & Adler, R. F. Spatial patterns of global precipitation change and variability during 1901–2010. *J. Clim.* **28**, 4431–4453 (2015).
81. Santer, B. D. et al. Identification of human-induced changes in atmospheric moisture content. *Proc. Natl Acad. Sci. USA* **104**, 15248–15253 (2007).
82. O'Gorman, P. & Muller, C. J. How closely do changes in surface and column water vapor follow Clausius–Clapeyron scaling in climate change simulations? *Environ. Res. Lett.* **5**, 025207 (2010).
83. Wentz, F. J. & Schabel, M. Precise climate monitoring using complementary satellite data sets. *Nature* **403**, 414–416 (2000).
84. Trenberth, K. E., Fasullo, J. & Smith, L. Trends and variability in column-integrated atmospheric water vapor. *Clim. Dyn.* **24**, 741–758 (2005).
85. Chung, E.-S., Soden, B., Sohn, B. & Shi, L. Upper-tropospheric moistening in response to anthropogenic warming. *Proc. Natl Acad. Sci. USA* **111**, 11636–11641 (2014).
86. Wang, J., Dai, A. & Mears, C. Global water vapor trend from 1988 to 2011 and its diurnal asymmetry based on GPS, radiosonde, and microwave satellite measurements. *J. Clim.* **29**, 5205–5222 (2016).
87. Allen, M. R. & Ingram, W. J. Constraints on future changes in climate and the hydrologic cycle. *Nature* **419**, 228–232 (2002).
88. Andrews, T., Forster, P. M., Boucher, O., Bellouin, N. & Jones, A. Precipitation, radiative forcing and global temperature change. *Geophys. Res. Lett.* **37**, L14701 (2010).
89. Samset, B. et al. Fast and slow precipitation responses to individual climate forcers: A PDRMIP multimodel study. *Geophys. Res. Lett.* **43**, 2782–2791 (2016).
90. Collins, M. et al. in *Climate Change 2013: The Physical Science Basis. Contribution of Working Group I to the Fifth Assessment Report of the Intergovernmental Panel on Climate Change* Ch. 12 (eds Stocker, T. F. et al.) 1029–1136 (Cambridge Univ. Press, 2013).
91. Greve, P. et al. Global assessment of trends in wetting and drying over land. *Nat. Geosci.* **7**, 716–721 (2014).
92. Byrne, M. P. & O'Gorman, P. A. The response of precipitation minus evapotranspiration to climate warming: Why the "wet-get-wetter, dry-get-drier" scaling does not hold over land. *J. Clim.* **28**, 8078–8092 (2015).
93. Yang, T., Ding, J., Liu, D., Wang, X. & Wang, T. Combined use of multiple drought indices for global assessment of dry gets drier and wet gets wetter paradigm. *J. Clim.* **32**, 737–748 (2019).
94. Westra, S., Alexander, L. V. & Zwiers, F. W. Global increasing trends in annual maximum daily precipitation. *J. Clim.* **26**, 3904–3918 (2013).
95. Fowler, H. J. et al. Anthropogenic intensification of short-duration rainfall extremes. *Nat. Rev. Earth Environ.* **2**, 107–122 (2021).
96. Singh, H. K., Bitz, C. M., Donohoe, A., Nusbaumer, J. & Noone, D. C. A mathematical framework for analysis of water tracers. Part II: Understanding large-scale perturbations in the hydrological cycle due to CO_2 doubling. *J. Clim.* **29**, 6765–6782 (2016).
97. Trenberth, K. E., Dai, A., Rasmussen, R. M. & Parsons, D. B. The changing character of precipitation. *Bull. Am. Meteorol. Soc.* **84**, 1205–1218 (2003).
98. Dacre, H. F., Clark, P. A., Martinez-Alvarado, O., Stringer, M. A. & Lavers, D. A. How do atmospheric rivers form? *Bull. Am. Meteorol. Soc.* **96**, 1243–1255 (2015).
99. Hu, H. & Dominguez, F. Understanding the role of tropical moisture in atmospheric rivers. *J. Geophys. Res. Atmos.* **124**, 13826–13842 (2019).
100. McDonnell, J. J. Beyond the water balance. *Nat. Geosci.* **10**, 396–396 (2017).
101. McGuire, K. J. & McDonnell, J. J. A review and evaluation of catchment transit time modeling. *J. Hydrol.* **330**, 543–563 (2006).
102. Brooks, J. R., Barnard, H. R., Coulombe, R. & McDonnell, J. J. Ecohydrologic separation of water between trees and streams in a Mediterranean climate. *Nat. Geosci.* **3**, 100–104 (2010).
103. Kirchner, J. W., Feng, X. & Neal, C. Fractal stream chemistry and its implications for contaminant transport in catchments. *Nature* **403**, 524–527 (2000).
104. Godsey, S. E. et al. Generality of fractal 1/f scaling in catchment tracer time series, and its implications for catchment travel time distributions. *Hydrol. Proc.* **24**, 1660–1671 (2010).
105. Held, I. M. & Soden, B. J. Water vapor feedback and global warming. *Annu. Rev. Energy Environ.* **25**, 441–475 (2000).
106. Schneider, T., O'Gorman, P. A. & Levine, X. J. Water vapor and the dynamics of climate changes. *Rev. Geophys.* **48**, RG3001 (2010).
107. Arkin, P. A., Smith, T. M., Sapiano, M. R. & Janowiak, J. The observed sensitivixy of the global hydrological cycle to changes in surface temperature. *Environ. Res. Lett.* **5**, 035201 (2010).

108. Hersbach, H. et al. The ERA5 global reanalysis. *Q. J. R. Meteorol. Soc.* **146**, 1999–2049 (2020).
109. Risi, C. et al. Process-evaluation of tropospheric humidity simulated by general circulation models using water vapor isotopologues: 1. Comparison between models and observations. *J. Geophys. Res. Atmos.* **117**, D05303 (2012).
110. Huffman, G. J., Stocker, E. F., Bolvin, D. T., Nelkin, E. J. &Tan, J. GPM IMERG Final Precipitation L3 1 day 0.1 degree x 0.1 degree V06. (Goddard Earth Sciences Data and Information Services Center, 2019).
111. Wentz, F. J., Ricciardulli, L., Hilburn, K. & Mears, C. How much more rain will global warming bring? *Science* **317**, 233–235 (2007).

Acknowledgements
L.G., R.N. and J.E.-B. were funded by the Spanish government within the LAGRIMA (RTI2018-095772-B-I00) project, funded by Ministerio de Ciencia, Innovación y Universidades, Spain, which are also funded by FEDER (European Regional Development Fund, ERDF). J.E.-B. was also supported by the Xunta de Galicia (Galician Regional Government) under grant ED481B 2018/069 and by the Fulbright Program (US Department of State). L.G., R.N. and J.E.-B. were partially supported by Xunta de Galicia, Spain under project ED413C 2017/64 'Programa de Consolidacion e Estructuracion de Unidades de Investigacion Competitivas (Grupos de Referencia Competitiva)' co-funded by the European Regional Development Fund, European Union (FEDER). J.E.-B. thanks the Defense University Center at the Spanish Naval Academy (CUD-ENM) for all the support provided for this research. R.V.d.E. acknowledges funding from the Netherlands Organization for Scientific Research (NWO), project number 016.Veni.181.015. A.M.D.-Q. acknowledges support from IAEA CRP F31006 (UCR project number B9519). F.D. is supported by National Science Foundation (NSF) CAREER Award AGS 1454089. H.S. acknowledges support by the Norwegian Research Council (Project SNOWPACE, grant no. 262710) and by the European Research Council (Consolidator Grant ISLAS, project no. 773245).

Author contributions
L.G. initiated writing of the Review and organized the writing process. All the authors contributed equally to the discussion and writing of the manuscript.

Competing interests
The authors declare no competing interests.

Peer review information
Nature Reviews Earth & Environment thanks M. Byrne, Z. Wei and Ø. Hodnebrog for their contribution to the peer review of this work.